INORGANIC CHEMISTRY FRONTIERS

RESEARCH ARTICLE

View Article Online
View Journal | View Issue

Cite this: *Inorg. Chem. Front.*, 2024, **11**, 3618

Achieving strong second harmonic generation effects induced *via* dimensional increase of PbX_6 octahedra and halogen substitutes in $(C_{10}H_{11}N_3)PbX_4$ (X = Cl or Br)†

Li-Ling Zhang,[a] Qingran Ding, *[a] Peihan Wang,[b] Yanqiu Zhang,[a] Qing-Yan Liu, *[a] Yu-Ling Wang *[a] and Junhua Luo[a,c]

Obtaining noncentrosymmetric structures and achieving desired performance indicators in nonlinear optics (NLO) are ongoing challenges. In this work, the rational design of an A-site cation (di(pyridin-4-yl) amine cation, $[C_{10}H_{11}N_3]$), stereochemically active lone pair cation (Pb^{2+}) and halogen substitutes in hybrid metal halide perovskites (ABX_3) was utilized to obtain two novel NLO crystals, $(C_{10}H_{11}N_3)PbX_4$ (X = Cl or Br), achieving desirable NLO performance, including pronounced anisotropy of second harmonic generation (SHG). Through the introduction of PbX_6 octahedrons in the $(C_{10}H_{11}N_3)BX_4$ system, compounds transformed from zero-dimensional to one-dimensional structures, resulting in significantly enhanced SHG activity. By controlling the halogen atoms, the SHG effect and birefringence of $(C_{10}H_{11}N_3)PbX_4$ were further improved. Experimental and theoretical studies validated that the improved NLO performance in the $(C_{10}H_{11}N_3)PbX_4$ system is closely related to the modulation of the octahedral distortion of PbX_6. The successful utilization of such structural dimension evolution and halogen substitution strategy offers a universal way for the rational regulation of crystal structures and optoelectronic performance of hybrid metal halide perovskites.

Received 2nd April 2024,
Accepted 6th May 2024

DOI: 10.1039/d4qi00832d

rsc.li/frontiers-inorganic

Introduction

Hybrid metal halide perovskites have been widely utilized in many fields such as photodetectors, light-emitting diodes, and solar cells.[1–4] Their excellent optical properties and diverse structural modifiability make them an ideal choice in research on optoelectronic devices.[5,6] In the past years, hybrid metal halide perovskites have also attracted significant attention in the technology field of nonlinear optics.[7] Their excellent optical properties make them potential candidates for nonlinear optical (NLO) applications,[8–11] thus becoming one of the research hotspots. To explore the potential application of hybrid metal perovskite materials in the field of nonlinear optics, it is the prerequisite to obtain compounds with crystallographically noncentrosymmetric structures. Additionally, second harmonic generation (SHG) response (comparable to or larger than that of potassium dihydrogen phosphate (KDP)) and birefringence (~0.07) are widely used as critical performance indicators for evaluating materials in this field.[12] Thus, it is an ongoing challenge to design and synthesize NLO crystals with excellent comprehensive properties.

Based on the typical ABX_3 chemical formula of metal halide perovskites, it is possible to achieve a noncentrosymmetric structure and further optimize its performance through three aspects: A-site, B-site, and X-site. When designing the B-site to obtain a noncentrosymmetric structure, a successful approach involves introducing one stereochemically active lone pair (SCALP) cation (Pb^{2+}, Bi^{3+}, Sn^{2+}, Sb^{3+}, *etc.*).[13–17] This strategy has been successfully employed for various NLO crystals, such as $SbI_3{\cdot}(S_8)_3$,[18] $BiO(IO_3)$,[19] $MB_2O_3F_2$ (M = Sn or Pb),[20] $LiHgPO_4$,[21] and Pb_2BO_3Cl.[22] By incorporating SCALP cations, it is possible to further optimize SHG response and birefringence, which are observed in SbB_3O_6,[23] $Pb_2BO_3NO_3$,[24] $Sn_2B_5O_9Cl$,[25] $Rb_2SbC_2O_4Cl_3$,[26] *etc*. When evaluating the influence of halide anions on the X-site, it is widely acknowledged that these anions exhibit a descending trend in terms of their contribution

[a]*College of Chemistry and Chemical Engineering, Key Lab of Fluorine and Silicon for Energy Materials and Chemistry of Ministry of Education and National Engineering Research Centre for Carbohydrate Synthesis, Jiangxi Normal University, Nanchang 330022, China. E-mail: dqr@jxnu.edu.cn, qyliuchem@jxnu.edu.cn, ylwang@jxnu.edu.cn*

[b]*School of Materials Science and Engineering, Frontiers Science Center for New Organic Matter, Nankai University, Tianjin 300350, China*

[c]*State Key Laboratory of Structural Chemistry, Fujian Institute of Research on the Structure of Matter, Chinese Academy of Sciences, Fuzhou 350002, China*

†Electronic supplementary information (ESI) available. CCDC 2310909 and 2310914. For ESI and crystallographic data in CIF or other electronic format see DOI: https://doi.org/10.1039/d4qi00832d

to SHG efficiency, *i.e.* I > Br > Cl.[27–30] Despite the significant achievements yielded by the above-mentioned strategies, there are still limitations in modulating the physicochemical properties of the hybrid metal halide perovskite family.

The rational design of A-site cations may be a more effective strategy to achieve desirable performance. Extensive investigations have been carried out by scientists, yielding remarkable achievements, including quasi-spherical theory for molecular ferroelectrics.[31–33] Regarding the design of SHG crystals, Mao has reported that controlling the A-site cation enhances the SHG response in the $AGeBr_3$ perovskite structure.[34] When it comes to the design of anisotropic crystals, Zhao *et al.* utilized organic π-conjugated cyclic cations (similar to π-conjugated $[B_3O_6]^{3-}$ ring in α-BaB_2O_4) to effectively enhance the birefringence performance.[35,36] The birefringence values range from 0.275@1064 nm for $CsPbI_3$, 0.292@1064 nm for $(CH_3NH_3)PbI_3$,[37] and further increase to 0.322@550 nm for $(C_3N_6H_8)PbBr_4$,[36] and more recently to 0.42@550 nm for $(C_6N_{10}H_8)Pb_2Br_6$,[38] surpassing those of commercially available birefringent crystals such as α-BaB_2O_4 (0.122@532 nm)[39] and YVO_4 (0.204@532 nm).[40] When the A-site cation transforms from monocation Cs^+ to linear moiety $[CH_3NH_3]^+$, then to monocyclic $[C_3N_6H_8]^+$, and is ultimately modified into a tricyclic $[C_6N_{10}H_8]^+$ cation, the birefringence value gradually increases. Additionally, other monocyclic anions, such as $[HC_3N_3O_3]^{2-}$,[41] $[HC_3N_3S_3]^{2-}$,[42] $[H_2C_6N_9]^-$,[43] $[PO_2(NH)_3(CO)_2]^-$,[44] and tricyclic anion $[H_2C_6N_7O_3]^-$,[45] along with their sub-groups have been reported for their notable birefringence or NLO performance.

In this work, we employed a π-conjugated bicyclic organic cation of diprotonated di(pyridin-4-yl)amine, $[C_{10}H_{11}N_3]^{2+}$, as the A-site cation, the SCALP cation Pb^{2+} as the B-site cation and combining with the tuning of the halide atoms to obtain two novel NLO crystals, $(C_{10}H_{11}N_3)PbX_4$ (X = Cl(**1**) and Br(**2**)). Interestingly, by introducing the PbX_6 octahedral structure, the dimensionality of the compounds is transformed from zero-dimensional (0-D) $(C_{10}H_{11}N_3)_2SiF_6$ reported by our group[46] to the present one-dimensional (1-D) $(C_{10}H_{11}N_3)PbX_4$, thereby increasing their SHG effect from 1.2-fold that of KDP to 3.6 times that of KDP (corresponding to powder sample **1**). Moreover, by further controlling the halogen atoms, we successfully increased the SHG effect of the powder sample **2** to 4.3 times that of KDP. For the SHG intensity of the selected single crystal, the SHG intensity of crystal **1** is 3.8 times that of KDP. Again, crystal **2** exhibits an enhanced SHG intensity, which is 5 times that of KDP. The birefringence at 550 nm increased from 0.046 in **1** to 0.127 in **2**.

Results and discussion

Single crystals of $(C_{10}H_{11}N_3)PbX_4$ were successfully prepared by a facile aqueous solution method (ESI†). The powder X-ray diffraction patterns of the experimental samples agree well with the calculated results based on single-crystal X-ray diffraction analysis (Fig. S1†). The thermogravimetric analysis curves of both compounds reveal a decomposition temperature of 560 K (Fig. S2†).

Both $(C_{10}H_{11}N_3)PbCl_4$ (**1**) and $(C_{10}H_{11}N_3)PbBr_4$ (**2**) are crystallized in the monoclinic space group *Cc* (Table S1 in ESI†), which features a noncentrosymmetric structure. Due to their isomorphism, compound **2** is chosen here for the structural analysis. Compound **2** exhibits a 1-D chain structure, where $[C_{10}H_{11}N_3]$ (Fig. 1a) acts as the A-site cation filling between the

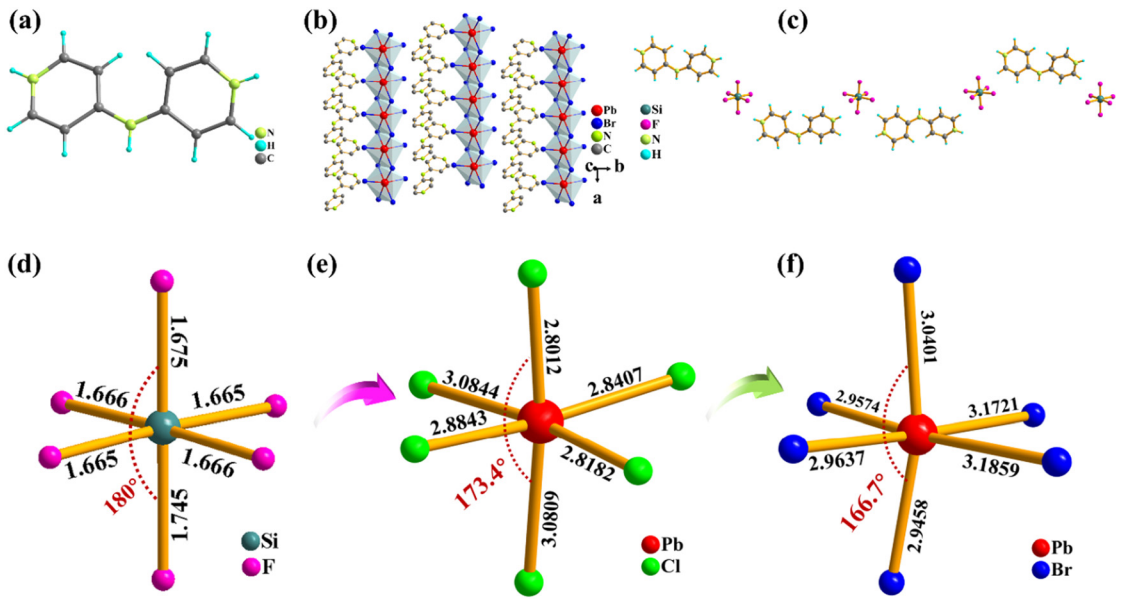

Fig. 1 (a) The structure of the organic cation $[C_{10}H_{11}N_3]^{2+}$. (b) 1-D chain structure of compound **2** (hydrogen atoms are omitted for clarity.). (c) Crystal structure of $(C_{10}H_{11}N_3)SiF_6$. (d) $[SiF_6]$ Octahedron in $(C_{10}H_{11}N_3)SiF_6$. (e) Distorted $[PbCl_6]$ octahedron in **1**. (f) Distorted $[PbBr_6]$ octahedron in **2**.

chains (Fig. 1b). In our reported $(C_{10}H_{11}N_3)_2SiF_6$, due to the unavailability of further Si–F–Si connection, it eventually forms a 0-D structure (Fig. 1c). However, in $(C_{10}H_{11}N_3)PbX_4$, the PbX_6 octahedra form an infinite array by linking to each other *via* edge-sharing (Fig. 1b). Such results suggest that the structural dimensionality of the $(C_{10}H_{11}N_3)BX_4$ system can be rationally regulated by the B-site. For **1**, the Pb–Cl bond lengths of the $PbCl_6$ octahedron vary from 2.8012 to 3.0844 Å and the Cl–Pb–Cl bond angles range from 90 to 96.567(5)° (Fig. 1e and Table S2†). For **2**, the Pb–Br distances of the $PbBr_6$ octahedron change from 2.9458 to 3.1859 Å, and the Br–Pb–Br bond angles change from 90 to 103.206(2)° (Fig. 1f and Table S3†). Obviously, the order of the distortion of the BX_6 octahedra is $PbBr_6$ > $PbCl_6$ > SiF_6. The distortion of BX_6 octahedra combined with the nonlinear configuration of $[C_{10}H_{11}N_3]^{2+}$ cations possesses electronic asymmetry in these compounds, which synergistically results in the NCS structures and the corresponding properties including the SHG activity. The organic and inorganic moieties in **1** and **2** are linked by the weak hydrogen bonds of N–H···X (X = Cl, Br) (Table S4†).

The optical photographs of the crystals of **1** and **2** are displayed in Fig. 2a. The optical absorption spectra for both compounds provide the band gaps of 3.35 eV for **1** and 2.95 eV for **2** (Fig. 2b). Considering that $(C_{10}H_{11}N_3)PbX_4$ crystallizes in NCS structures and the observed large distortion of $[PbX_6]$ moieties, it is expected to exhibit strong SHG activity. The SHG activity of the powder samples of $(C_{10}H_{11}N_3)PbX_4$ was recorded using the Kurtz and Perry method under 1064 nm laser irradiation and with KDP polycrystals as the reference. By comparing the SHG response of $(C_{10}H_{11}N_3)PbX_4$ and KDP in the same particle size range of 210–300 μm, it is found that **1** displays a relatively large SHG response, which is 3.6 times that of KDP (Fig. 2c). In addition, **2** exhibits a more larger SHG response, which is 4.3 times that of KDP. The crystal structures of $(C_{10}H_{11}N_3)PbX_4$ are regulated by different halogens of X (X = Cl, Br), leading to stronger SHG activity of the bromide one as compared to the chloride one. Such enhanced SHG activity can be ascribed to the longer Pb–Br bond distances and larger distortion for $[PbBr_6]$ octahedra in **2**. Obviously, as compared to **1**, the larger distortion of $[PbBr_6]$ octahedra leads to a larger total macroscopic dipolar moment for **2**, thus endowing an enhanced SHG intensity for **2**. Furthermore, the phase-matching experiments based on the polycrystal samples with different particle sizes were carried out. As depicted in Fig. 2d, the SHG intensities of the two compounds gradually increase with the increasing particle size and achieve saturation with a size larger than 200 μm. Such an evolution suggests that both are phase-matching NLO materials. The strong SHG activity and phase-matchable behavior for the present NLO materials make them promising for applications in NLO devices. It should be noted that the SHG response of the present $(C_{10}H_{11}N_3)PbX_4$ is significantly higher than that of the majority of the organic–inorganic hybrid metal halides, including (R/S-2-MPD)$PbBr_3$ (1.4 × KDP),[47] (R/S-3-aminopiperidine)PbI_4 (2.1 × KDP),[48] (R/S-3-aminopiperidine)$SbCl_5$ (1.93 × KDP),[49] and $(C_4H_{10}NO)PbBr_3$ (0.81 × KDP).[50]

In addition to the SHG activities of the powder samples, the detailed SHG properties of the single-crystals for $(C_{10}H_{11}N_3)PbX_4$ were further measured on a femtosecond laser installation[51] in a reflection geometry with incidence and detection angles being 45°. As shown in Fig. 3a and S3,† the resulting spectra of $(C_{10}H_{11}N_3)PbX_4$ single-crystals show clear SHG activities upon excitation with the laser wavelengths varying from 820 to 1040 nm. Similar to the trend of SHG intensity of the powder samples, the SHG intensity of crystal **2** is about 1.3 times that of crystal **1** and 5 times that of the KDP crystal excited at the laser wavelength of 1040 nm (Fig. 3b). Such an increase in SHG intensity for crystal **2** could be a result of the

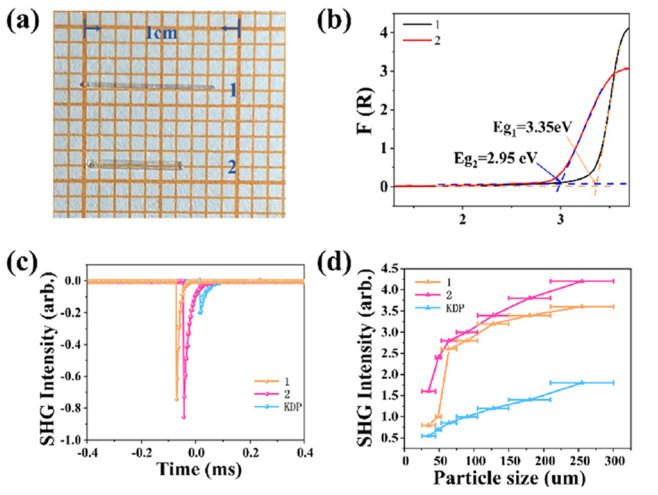

Fig. 2 (a) Photographs of crystals of **1** and **2**. (b) The band-gap values of **1** and **2**. (c) SHG intensities of **1**, **2** and KDP. (d) SHG intensities of **1**, **2** and KDP with different particle sizes.

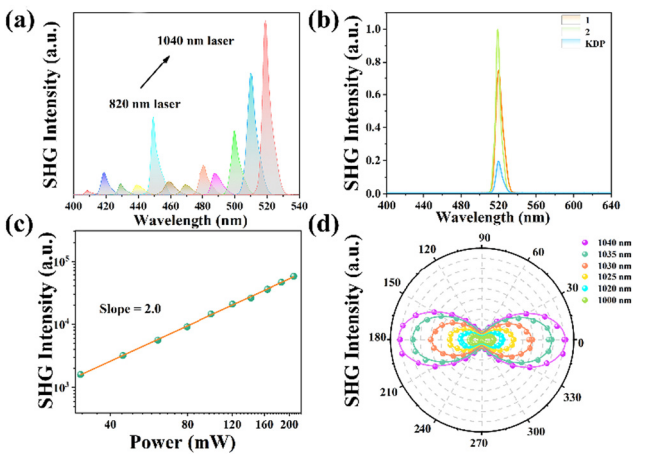

Fig. 3 (a) SHG response of crystal **2** pumped at different wavelengths. (b) SHG intensity of crystals **1**, **2** and KDP pumped at 1040 nm laser. (c) Logarithmic plot of SHG intensity *versus* incident power for crystal **2** (the orange line is the best linear fitting of the experimental data). (d) SHG intensity of crystal **2** at different linearly polarized angles and different laser wavelengths (the solid lines are the nonlinear fitting of the experimental data).

enhanced octahedral distortion[27,52] of [$PbBr_6$] in **2** in comparison to that of [$PbCl_6$] in **1**, emphasizing the important role of the halogen substitution. SHG images of single crystals **1** and **2** clearly demonstrate the profile of the rod-shaped crystals for **1** and **2** (Fig. S4†).

Additionally, the confirmation of the second-order nonlinear optics process is demonstrated by the quadratic scaling of SHG intensity with the incident power for both crystals (Fig. 3c and S5†). Fig. 3d shows the SHG intensity of crystal **2** at different linearly polarized angles with the laser wavelengths of 1040, 1035, 1030, 1025, 1020, and 1000 nm. The resulting dumbbell-shaped plots suggest the notable anisotropy of the SHG response and dipolar polarization for **2**, which shows the strongest SHG response at angles of 0 and 180°, and the weakest SHG response at angles of 90 and 270°. The polarization-dependent plots for crystal **1** show similar dipolar profiles (Fig. S6†), again indicating the large anisotropy of its SHG intensity. The polarization ratio (ρ) calculated with the formula of $\rho = (I_{max} - I_{min})/(I_{max} + I_{min})$[30] can be determined to be 94.9% for **1** and 87.1% for **2**, respectively. The notable polarization ratios for **1** and **2** are comparable to those of hybrid metal halide perovskites such as [*S*-3-aminopiperidine]PbI_4 (83%),[48] (*R*-MBA)$CuBr_2$ (97.5%),[11] and $DMA_4[InCl_6]Br$ (99.9%),[30] highlighting the significant anisotropy of the SHG intensity for crystals **1** and **2**.

To achieve phase matching in NLO materials, it is crucial to have a moderate birefringence. Thus, transparent crystals **1** and **2** were selected for birefringence measurement using a cross-polarizing microscope with a quartz wedge compensator. The original crystals exhibit an orange interference color for **1** and blue for **2** (Fig. 4a and d) when observed under cross-polarized light. Subsequently, both crystals **1** and **2** achieve complete extinction (Fig. 4b and e) as the quartz wedge compensator rotated. Furthermore, the crystal thickness of **1** and **2**, as measured using the polarizing microscope, are 6.11 μm and 7.71 μm, respectively (Fig. 4c and f). Based on the formula: $\Delta n = R/d$, the birefringence is determined to be 0.046 for **1** at a wavelength of 550 nm. Crystal **1** has a moderate birefringence, which is comparable to that of some noted NLO materials, such as LiB_3O_5 (0.040)[53] and $CsLiB_6O_{10}$ (0.049)[54] at a wavelength of 500 nm. It was observed that the birefringence of crystal **2** increased to 0.127 under the same conditions, a considerable enhancement compared to that in crystal **1**. Detailed analyses attributed this to the pronounced effects of halogen substitution, which not only caused an increment in the Pb–X bond lengths (from Pb–Cl to Pb–Br) but also intensified the distortion of the PbX_6 octahedra. More specifically, the X–Pb–X bond angles at the octahedral symmetry axes have shifted from 173.4° (with Cl atoms) to 166.7° (with Br atoms) (Fig. 1e and f). The resultant changes in the structural parameters exert significant impacts on the optical characteristics of the crystals, in particular, their birefringence when subjected to light propagation. For a better understanding of the improvement in birefringence for **2**, the local dipole moments for $PbCl_6$ and $PbBr_6$ structural units are calculated with a bond-valence approach.[55] The net dipole moment for a PbX_6 octahedron can be obtained from the vector sum of the dipole moments of the six Pb–X bonds. The calculated results giving the net dipole moments for $PbCl_6$ and $PbBr_6$ octahedrons are 5.26 and 13.58 Debye (Fig. S7†), respectively. The dipole moment vectors for both octahedrons are directed towards a triangular face of the octahedrons. The larger net dipole moment for the $PbBr_6$ structural units and the parallel arrangement of the $PbBr_6$ octahedrons in the 1-D chains are beneficial to generate the enhanced birefringence for **2**.

To further corroborate the observed birefringence phenomena, we employed the first-principles method to theoretically predict the birefringence of crystals **1** and **2** at a wavelength of 550 nm, yielding calculated values of 0.041 and 0.121, respectively (Fig. 5a and b). The high concordance between the theoretical values and the experimentally measured ones confirms the reliability of the birefringence effects we have recorded. In order to investigate the origin of SHG for **1** and **2**, theoretical calculations were performed using density func-

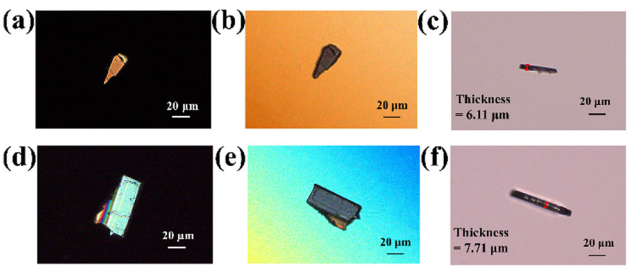

Fig. 4 (a) Original interference color of crystal **1** under orthogonal polarized light. (b) Crystal **1** under complete extinction. (c) Thickness of the measured crystal **1**. (d) Original interference color of crystal **2** under orthogonal polarized light. (e) Crystal **2** under complete extinction. (f) Thickness of the measured crystal **2**.

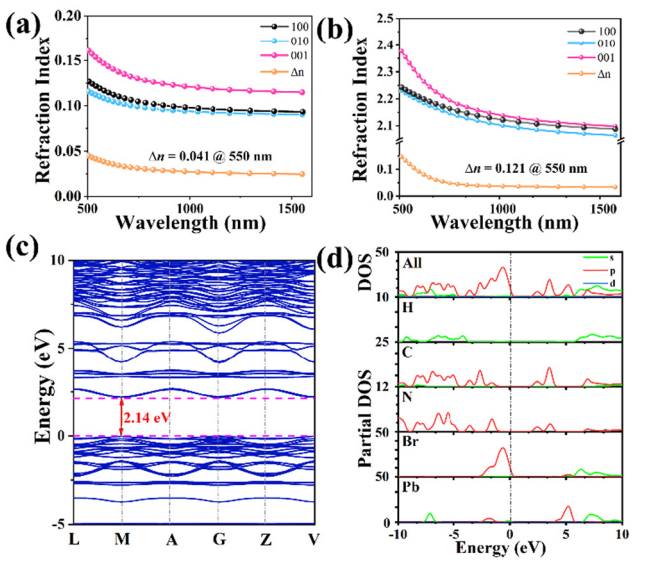

Fig. 5 The wavelength-dependent refractive indices of (a) compound **1** and (b) **2**. (c) Calculated energy band structures of compound **2**. (d) DOS and PDOS of compound **2**.

tional theory (DFT) methods. The results of the theoretical calculations revealed that the direct band gaps of compounds **1** and **2** are estimated to be 2.27 eV and 2.14 eV (Fig. 5c and S8†), respectively. The calculated band gaps are in agreement with the experimentally determined values illustrated in Fig. 2b. The total density of states (DOS) and partial DOS (PDOS) were calculated to explore the origin of the NLO activity. Based on the PDOS results shown in Fig. 5d, compound **2** exhibits a concentration of C 2p, H 1s, N 2p, Pb 6p, and Br 4p states within the energy range from −5 to 5 eV, approaching the Fermi level. Specifically, the valence band maximum of compound **2** is primarily occupied by Br 4p, C 2p, and N 2p states, with minor contributions from Pb 6p and H 1s. The conduction band minimum is mainly formed by Pb 6p, C 2p, and N 2p states. Similarly, compound **1** exhibits a similar trend (Fig. S9†). Overall, the band gaps and SHG properties of compounds **1** and **2** are predominantly influenced by the distortion of the [PbX_6] octahedron in the inorganic framework and the dipolar π-conjugated bi-cyclic organic cation [$C_{10}H_{11}N_3$].

Conclusions

In summary, we successfully utilized [$C_{10}H_{11}N_3$] as the A-site cation, the SCALP cation Pb^{2+} as the B-site cation, and combined with the tuning of halide atoms to synthesize two novel nonlinear optical crystals, namely, ($C_{10}H_{11}N_3$)PbX_4 (X = Cl, Br). The structural dimensionality of the ($C_{10}H_{11}N_3$)BX_4 compounds can be elaborately regulated by the B-site cation, thus achieving pronounced enhancement of the SHG response. The introduction of PbX_6 octahedra enabled the control of dimensionality and the enhancement of SHG and birefringence in both compounds. Specifically, by modulating the octahedral distortion of PbX_6, the SHG response increased from 3.8 to 5 times that of KDP, while the birefringence increased from 0.046 for **1** to 0.127 for **2**, which are comparable to those of commercial birefringent crystals. Theoretical calculations further confirmed the origin of these performance improvements. Furthermore, significant anisotropy of the SHG intensity and dipolar polarization were observed for crystals **1** and **2**. The results of this study effectively demonstrated the crystal structures and outstanding SHG effects of these novel compounds, providing an effective approach for the development of high-performance NLO crystals. Such structural dimensional evolution and halogen substitution approaches are expected to be useful ways to rationally modulate the crystal structures and optoelectronic properties of the hybrid metal halide perovskites for diverse device applications.

Experimental

Materials and Instrumentations

All chemical reagents and solvents were commercially available and used without further purification. Crystal diffraction data of **1** and **2** were collected on a Rigaku Oxford SuperNova diffractometer. The crystallographic data are presented in Table S1 (ESI†). CIF for **1** and **2** have been deposited in the Cambridge Crystallographic Data Centre, CCDC numbers are 2310909 and 2310914 for **1** and **2**, respectively.

Powder second-harmonic generation measurements were carried out by the Kurtz–Perry method. The measurements were performed using a Q-switched Nd:YGA laser at a wavelength of 1064 nm. The SHG measurements of single crystals were carried out using a multiphoton nonlinear optical microscope system. A commercial femtosecond pump (Mai Tai HP, wavelength ranging from 690 to 1040 nm) was used in the reflection geometry with incidence and detection angles both 45 degrees. The linearly polarized pump was altered with the $\lambda/2$ plate. The reflected SHG signal was received from the front surface of the crystals. The linearly polarized dependent SHG signals were collected every 10 degrees. The KDP was used as a benchmark for SHG signal intensity. The Birefringence of ($C_{10}H_{11}N_3$)PbX_4 (X = Cl, Br) was obtained using a polarizing microscope (Nikon LV1000) equipped with a Berek compensator at a wavelength of 550 nm. The detailed experimental methods are provided in the ESI.†

Syntheses

Synthesis of ($C_{10}H_{11}N_3$)$PbCl_4$ (1). $PbCl_2$ (0.069 g, 0.25 mmol) and di(pyridin-4-yl)amine (0.043 g, 0.25 mmol) were dissolved in 4 mL hydrochloric acid and stirred for 3 h at 100 °C. The crystals of ($C_{10}H_{11}N_3$)$PbCl_4$ were obtained by slowly evaporating the clear resultant solution at room temperature after a day. The yield was calculated at 65%. Main IR spectra (cm^{-1}, KBr pellet): 3718 (m), 3045 (s), 1612 (s), 1485(s), 1352 (s), 1192 (s), 1092 (m), 998 (m), 779 (s), 678 (w). Elemental analysis for $C_{10}H_{11}N_3Cl_4Pb$ (522.21) (calc/found: C, 22.99/23.01; H, 2.12/2.16; N, 8.04/8.01).

Synthesis of ($C_{10}H_{11}N_3$)$PbBr_4$ (2). $PbBr_2$ (0.11 g, 0.3 mmol) and di(pyridin-4-yl)amine (0.051 g, 0.3 mmol) were dissolved in 4 mL hydrobromic acid and stirred for 3 h at 130 °C. The crystals of ($C_{10}H_{11}N_3$)$PbBr_4$ were obtained by slowly evaporating the clear resultant solution at room temperature after a day. The yield was calculated at 68%. Main IR spectra (cm^{-1}, KBr pellet): 1625 (s), 1499(s), 1345 (s), 1179 (s), 1092 (m), 998 (m), 905 (m), 785 (s), 685 (m). Elemental analysis for $C_{10}H_{11}N_3Br_4Pb$ (700.05) (calc/found: C, 17.15/17.16; H, 1.58/1.61; N, 6.00/6.04).

Author contributions

Li-Ling Zhang: Investigation, data curation, formal analysis, writing – original draft. Qingran Ding: Methodology, writing – original draft. Peihan Wang: Data curation. Yanqiu Zhang: Data curation. Qing-Yan Liu: Methodology, supervision, funding acquisition, writing – review and editing. Yu-Ling Wang: Conceptualization, supervision, funding acquisition, writing – review and editing. Junhua Luo: Validation.

Conflicts of interest

There are no conflicts to declare.

Acknowledgements

The authors thank the National Natural Science Foundation of China (22261023, 22361021 and 22201110) for the financial support.

References

1 Y. Liu, Z. Yang and S. Liu, Recent Progress in Single–Crystalline Perovskite Research Including Crystal Preparation, Property Evaluation, and Applications, *Adv. Sci.*, 2018, **5**, 1700471.
2 Z.-K. Tan, R. S. Moghaddam, M. L. Lai, P. Docampo, R. Higler, F. Deschler, M. Price, A. Sadhanala, L. M. Pazos, D. Credgington, F. Hanusch, T. Bein, H. J. Snaith and R. H. Friend, Bright Light-Emitting Diodes Based on Organometal Halide Perovskite, *Nat. Nanotechnol.*, 2014, **9**, 687–692.
3 G. Yang, J. Li, M. Wu, X. Yu and J. Yu, Recent Advances in Materials, Structures, and Applications of Flexible Photodetectors, *Adv. Electron. Mater.*, 2023, **9**, 2300340.
4 W. Yin, T. Shi and Y. Yan, Unique Properties of Halide Perovskites as Possible Origins of the Superior Solar Cell Performance, *Adv. Mater.*, 2014, **26**, 4653–4658.
5 H. Wang and D. H. Kim, Perovskite-Based Photodetectors: Materials and Devices, *Chem. Soc. Rev.*, 2017, **46**, 5204–5236.
6 W. Li, Z. Wang, F. Deschler, S. Gao, R. H. Friend and A. K. Cheetham, Chemically Diverse and Multifunctional Hybrid Organic–Inorganic Perovskites, *Nat. Rev. Mater.*, 2017, **2**, 16099.
7 Y. Zhou, Y. Huang, X. Xu, Z. Fan, J. B. Khurgin and Q. Xiong, Nonlinear Optical Properties of Halide Perovskites and Their Applications, *Appl. Phys. Rev.*, 2020, **7**, 041313.
8 W. Chen, F. Zhang, C. Wang, M. Jia, X. Zhao, Z. Liu, Y. Ge, Y. Zhang and H. Zhang, Nonlinear Photonics Using Low–Dimensional Metal–Halide Perovskites: Recent Advances and Future Challenges, *Adv. Mater.*, 2021, **33**, 2004446.
9 B. Liu, H. Zeng, X. Jiang and G. Guo, Phase Matching Achieved by Band Gap Widening in Infrared Nonlinear Optical Materials $[ABa_3Cl_2][Ga_5S_{10}]$ (A = K, Rb, Cs), *CCS Chem.*, 2020, **3**, 964–973.
10 J. Xu, X. Li, J. Xiong, C. Yuan, S. Semin, T. Rasing and X. Bu, Halide Perovskites for Nonlinear Optics, *Adv. Mater.*, 2020, **32**, 1806736.
11 F. Ge, B. Li, P. Cheng, G. Li, Z. Ren, J. Xu and X. Bu, Chiral Hybrid Copper(I) Halides for High Efficiency Second Harmonic Generation with a Broadband Transparency Window, *Angew. Chem., Int. Ed.*, 2022, **61**, e202115024.
12 P. Gong, L. Kang and Z. Lin, Realizing Deep-Ultraviolet Second Harmonic Generation by First-Principles-Guided Materials Exploration in Hydroxyborates, *J. Am. Chem. Soc.*, 2020, **142**, 15157–15163.
13 J. Chen, C. Hu, F. Mao, J. Feng and J. Mao, A Facile Route to Nonlinear Optical Materials: Three–Site Aliovalent Substitution Involving One Cation and Two Anions, *Angew. Chem., Int. Ed.*, 2019, **58**, 2098–2102.
14 L. Qi, Z. Chen, X. Shi, X. Zhang, Q. Jing, N. Li, Z. Jiang, B. Zhang and M.-H. Lee, $A_3BBi(P_2O_7)_2$ (A = Rb, Cs; B = Pb, Ba): Isovalent Cation Substitution to Sustain Large Second-Harmonic Generation Responses, *Chem. Mater.*, 2020, **32**, 8713–8723.
15 H. Yu, W. Zhang, J. Young, J. M. Rondinelli and P. S. Halasyamani, Bidenticity-Enhanced Second Harmonic Generation from Pb Chelation in $Pb_3Mg_3TeP_2O_{14}$, *J. Am. Chem. Soc.*, 2016, **138**, 88–91.
16 L. Bian, F. Cao and L. Li, Performance Improvement of Lead–Based Halide Perovskites through B–Site Ion–Doping Strategies, *Small*, 2023, **19**, 2302700.
17 M. Yan, H.-G. Xue and S.-P. Guo, Recent Achievements in Lone-Pair Cation-Based Infrared Second-Order Nonlinear Optical Materials, *Cryst. Growth Des.*, 2021, **21**, 698–720.
18 S.-P. Guo, Z.-D. Sun, Y. Chi and H.-G. Xue, Adduct-Type IR Nonlinear-Optical Crystal $SbI_3{\cdot}(S_8)_3$ with a Large Second-Harmonic Generation and a High Laser-Induced Damage Threshold, *Inorg. Chem.*, 2018, **57**, 11282–11288.
19 S. D. Nguyen, J. Yeon, S.-H. Kim and P. S. Halasyamani, $BiO(IO_3)$: A New Polar Iodate That Exhibits an Aurivillius-Type $(Bi_2O_2)^{2+}$ Layer and a Large SHG Response, *J. Am. Chem. Soc.*, 2011, **133**, 12422–12425.
20 M. Luo, F. Liang, Y. Song, D. Zhao, N. Ye and Z. Lin, Rational Design of the First Lead/Tin Fluorooxoborates $MB_2O_3F_2$ (M=Pb, Sn): Containing Flexible Two-Dimensional $[B_6O_{12}F_6]_\infty$ Single Layers with Widely Divergent Second Harmonic Generation Effects, *J. Am. Chem. Soc.*, 2018, **140**, 6814–6817.
21 B.-L. Wu, C.-L. Hu, F.-F. Mao, R.-L. Tang and J.-G. Mao, Highly Polarizable Hg^{2+} Induced a Strong Second Harmonic Generation Signal and Large Birefringence in $LiHgPO_4$, *J. Am. Chem. Soc.*, 2019, **141**, 10188–10192.
22 G. Zou, C. Lin, H. Jo, G. Nam, T. You and K. M. Ok, Pb_2BO_3Cl: A Tailor–Made Polar Lead Borate Chloride with Very Strong Second Harmonic Generation, *Angew. Chem., Int. Ed.*, 2016, **55**, 12078–12082.
23 Y. Liu, X. Liu, S. Liu, Q. Ding, Y. Li, L. Li, S. Zhao, Z. Lin, J. Luo and M. Hong, An Unprecedented Antimony(III) Borate with Strong Linear and Nonlinear Optical Responses, *Angew. Chem., Int. Ed.*, 2020, **59**, 7793–7796.
24 J. Song, C. Hu, X. Xu, F. Kong and J. Mao, A Facile Synthetic Route to a New SHG Material with Two Types of Parallel π–Conjugated Planar Triangular Units, *Angew. Chem., Int. Ed.*, 2015, **54**, 3679–3682.
25 J. Guo, A. Tudi, S. Han, Z. Yang and S. Pan, $Sn_2B_5O_9Cl$: A Material with Large Birefringence Enhancement Activated

Prepared via Alkaline–Earth–Metal Substitution by Tin, *Angew. Chem., Int. Ed.*, 2019, **58**, 17675–17678.
26 S. Han, A. Tudi, W. Zhang, X. Hou, Z. Yang and S. Pan, Recent Development of SnII, SbIII–based Birefringent Material: Crystal Chemistry and Investigation of Birefringence, *Angew. Chem., Int. Ed.*, 2023, **62**, e202302025.
27 Q. Shui, H. Tang, R. Fu, Y. Fang, Z. Ma and X. Wu, $Cs_3Pb_2(CH_3COO)_2X_5$ (X=I, Br): Halides with Strong Second–Harmonic Generation Response Induced by Acetate Groups, *Angew. Chem., Int. Ed.*, 2021, **60**, 2116–2119.
28 Y. Zheng, J. Xu and X. Bu, 1D Chiral Lead Halide Perovskites with Superior Second–Order Optical Nonlinearity, *Adv. Opt. Mater.*, 2022, **10**, 2101545.
29 D. Chen, S. Hao, L. Fan, Y. Guo, J. Yao, C. Wolverton, M. G. Kanatzidis, J. Zhao and Q. Liu, Broad Photoluminescence and Second-Harmonic Generation in the Noncentrosymmetric Organic–Inorganic Hybrid Halide $(C_6H_5(CH_2)_4NH_3)_4MX_7{\cdot}H_2O$ (M = Bi, In, X = Br or I), *Chem. Mater.*, 2021, **33**, 8106–8111.
30 J. Guan, Y. Zheng, P. Cheng, W. Han, X. Han, P. Wang, M. Xin, R. Shi, J. Xu and X. Bu, Free Halogen Substitution of Chiral Hybrid Metal Halides for Activating the Linear and Nonlinear Chiroptical Properties, *J. Am. Chem. Soc.*, 2023, **145**, 26833–26842.
31 H.-Y. Zhang, Y.-Y. Tang, P.-P. Shi and R.-G. Xiong, Toward the Targeted Design of Molecular Ferroelectrics: Modifying Molecular Symmetries and Homochirality, *Acc. Chem. Res.*, 2019, **52**, 1928–1938.
32 C. Chen, X. Zhao, Y. Gong, Y. Liu, Z. Chen, L. Zhang, J. Chen, Z. Deng, H. Lu, M. Luo, P. Canepa and L. Mao, Two-Dimensional Hybrid Dion–Jacobson Germanium Halide Perovskites, *Chem. Mater.*, 2023, **35**, 3265–3275.
33 M. R. Cerón, M. Izquierdo, N. Alegret, J. A. Valdez, A. Rodríguez-Fortea, M. M. Olmstead, A. L. Balch, J. M. Poblet and L. Echegoyen, Reactivity Differences of $Sc_3N@C_{2n}$ (2n = 68 and 80). Synthesis of the First Methanofullerene Derivatives of $Sc_3N@D_{5h}$-C_{80}, *Chem. Commun.*, 2016, **52**, 64–67.
34 Y. Liu, Y. Gong, S. Geng, M. Feng, D. Manidaki, Z. Deng, C. C. Stoumpos, P. Canepa, Z. Xiao, W. Zhang and L. Mao, Hybrid Germanium Bromide Perovskites with Tunable Second Harmonic Generation, *Angew. Chem., Int. Ed.*, 2022, **61**, e202208875.
35 J. Liu, X. He, G. Zhou, C. Xia, S. Zhou and J. Xu, Growth of Beta Barium Borate (β-BaB_2O_4) Thin Films on Alpha Barium Borate (α-BaB_2O_4) Substrates, *J. Cryst. Growth*, 2005, **277**, 359–363.
36 W. Huang, X. Zhang, Y. Li, Y. Zhou, X. Chen, X. Li, F. Wu, M. Hong, J. Luo and S. Zhao, A Hybrid Halide Perovskite Birefringent Crystal, *Angew. Chem., Int. Ed.*, 2022, **61**, e202202746.
37 T. Tong, M.-H. Lee and J. Zhang, Transformation of Optical Anisotropy Origins in Perovskite-Related Materials: A First-Principles Study, *J. Phys. Chem. C*, 2019, **123**, 31167–31174.
38 Q. Xu, W. Huang, H. Wang, Y. Li, Y. Zhou, L. Hou, S. Zhao and J. Luo, Designing a Dimension Reduced Hybrid Perovskite with Robust Large Birefringence by Expanding Cationic π–Delocation, *Small*, 2023, **19**, 2304333.
39 G. Zhou, J. Xu, X. Chen, H. Zhong, S. Wang, K. Xu, P. Deng and F. Gan, Growth and Spectrum of a Novel Birefringent α-BaB_2O_4 Crystal, *J. Cryst. Growth*, 1998, **191**, 517–519.
40 H. T. Luo, T. Tkaczyk, E. L. Dereniak, K. Oka and R. Sampson, High Birefringence of the Yttrium Vanadate Crystal in the Middle Wavelength Infrared, *Opt. Lett.*, 2006, **31**, 616–618.
41 X. Meng, F. Liang, K. Kang, J. Tang, T. Zeng, Z. Lin and M. Xia, Facile Growth of an Ultraviolet Hydroisocyanurate Crystal with Strong Nonlinearity and a Wide Phase-Matching Region from π-Conjugated $(HC_3N_3O_3)^{2-}$ Groups, *Inorg. Chem.*, 2019, **58**, 11289–11293.
42 M. Li, X. Zhang, Z. Xiong, Y. Li, Y. Zhou, X. Chen, Y. Song, M. Hong, J. Luo and S. Zhao, A Hybrid Antiperovskite with Strong Linear and Second–Order Nonlinear Optical Responses, *Angew. Chem., Int. Ed.*, 2022, **61**, e202211151.
43 Y. Li, X. Zhang, Y. Zhou, W. Huang, Y. Song, H. Wang, M. Li, M. Hong, J. Luo, S. Zhao, A. Yonezu, R. Krishna, G. Liu, J. Duan, R. Matsuda, W. Jin and B.-L. Chen, An Optically Anisotropic Crystal with Large Birefringence Arising from Cooperative π Orbitals, *Angew. Chem., Int. Ed.*, 2022, **61**, e202208811.
44 X. Song, Z. Du, B. Ahmed, Y. Li, Y. Zhou, Y. Song, W. Huang, J. Zheng, J. Luo and S. Zhao, A UV Solar-Blind Nonlinear Optical Crystal with Confined π-Conjugated Groups, *Inorg. Chem. Front.*, 2023, **10**, 5462–5467.
45 Y. Li, W. Huang, Y. Zhou, X. Song, J. Zheng, H. Wang, Y. Song, M. Li, J. Luo and S. Zhao, A High–Performance Nonlinear Optical Crystal with a Building Block Containing Expanded π–Delocalization, *Angew. Chem., Int. Ed.*, 2023, **62**, e202215145.
46 Z.-X. Chen, Y.-L. Wang and Q.-Y. Liu, A Hydrogen-Bonded Inorganic-Organic Network with Noncentrosymmetric Structure Exhibiting Second-Order Nonlinear Optical Response, *Inorg. Chem. Commun.*, 2018, **98**, 150–153.
47 Y. Zheng, J. Xu and X. Bu, 1D Chiral Lead Halide Perovskites with Superior Second–Order Optical Nonlinearity, *Adv. Opt. Mater.*, 2022, **10**, 2101545.
48 D. Fu, J. Xin, Y. He, S. Wu, X. Zhang, X. Zhang and J. Luo, Chirality–Dependent Second–Order Nonlinear Optical Effect in 1D Organic–Inorganic Hybrid Perovskite Bulk Single Crystal, *Angew. Chem., Int. Ed.*, 2021, **60**, 20021–20026.
49 S. Qi, P. Cheng, X. Han, F. Ge, R. Shi, L. Xu, G. Li and J. Xu, Organic–Inorganic Hybrid Antimony(III) Halides for Second Harmonic Generation, *Cryst. Growth Des.*, 2022, **22**, 6545–6553.
50 C. Shen, D. Sun, Y. Dang, K. Wu, T. Xu, R. Hou, H. Chen, J. Wang and D. Wang, $(C_4H_{10}NO)PbX_3$ (X = Cl, Br): Design of Two Lead Halide Perovskite Crystals with Moderate Nonlinear Optical Properties, *Inorg. Chem.*, 2022, **61**, 16936–16943.
51 C. Yuan, X. Li, S. Semin, Y. Feng, T. Rasing and J. Xu, Chiral Lead Halide Perovskite Nanowires for Second-Order Nonlinear Optics, *Nano Lett.*, 2018, **18**, 5411–5417.
52 X. Dong, L. Huang, H. Zeng, Z. Lin, K. M. Ok and G. Zou, High–Performance Sulfate Optical Materials Exhibiting

Giant Second Harmonic Generation and Large Birefringence, *Angew. Chem., Int. Ed.*, 2022, **61**, e202116790.
53 Q. Wang, F. Yang, X. Wang, J. Zhou, J. Ju, L. Huang, D. Gao, J. Bi and G. Zou, Deep-Ultraviolet Mixed-Alkali-Metal Borates with Induced Enlarged Birefringence Derived from the Structure Rearrangement of the LiB_3O_5, *Inorg. Chem.*, 2019, **58**, 5949–5955.
54 Y. Mori, I. Kuroda, S. Nakajima, T. Sasaki and S. Nakai, New Nonlinear Optical Crystal: Cesium Lithium Borate, *Appl. Phys. Lett.*, 1995, **67**, 1818–1820.
55 P. A. Maggard, T. S. Nault, C. L. Stern and K. R. Poeppelmeier, Alignment of acentric $MoO_3F_3^{3-}$ anions in a polar material: $(Ag_3MoO_3F_3)(Ag_3MoO_4)Cl$, *J. Solid State Chem.*, 2003, **175**, 27–33.